Exp. Theo. NANOTECHNOLOGY 3 (2019) 95-101 https://doi.org/10.56053/3.1.95

ZnO nanowire arrays for UV photodetector

J.A. Pyon, J. Yamaha, C. Cheroke*

Materials Science Division, Kyoto University, Kumatori-cho, Sennan-gun, Osaka 590-0494, Japan
*) Email: japyon@rri.kyoto-u.ac.jp

Received 14/7/2018, *Accepted* 14/11/2018, *Accepted* 15/1/2019

Well-crystallized ZnO nanowire arrays were grown on GaN/sapphire by one-step chemical vapor deposition under control of the fabrication pressure of 1000– 2500 Pa and the best-aligned arrays were obtained at 1000 Pa. A photoluminescence study shows a red shift with nanowire diameter increase. Under 365-nm UV irradiation of 0.3 mW/cm2, the photoresponse study of the best ZnO ar- rays shows an ultra-fast tri-exponential rise with three constants of 0.148, 0.064 and 0.613 s, and a bi-exponential de- cay behavior with two recovery constants of 30 and 270 ms. The ZnO/GaN heterojunction barriers could be responsible for the ultra-fast tri-exponential rise and bi-exponential de- cay behavior.

Keywords: ZnO; Array; UV.

1. INTRODUCTION

Recently, one-dimensional (1D) nanostructures have attracted increasing attention for a great variety of potential applications in nanodevices [1–3]. ZnO, one of the most important metal oxides, has a wide band gap of 3.37 eV and a high exciton binding energy of 60 meV at room temperature. One-dimensional ZnO nanostructures such as nanowires (NWs), nanorods, nanotubes, nanobelts, thin films etc. are extensively studied for their applications in various opto- electronic devices, e.g. light-emitting diodes (LEDs), solar cells, phototransistors, UV photodetectors etc. [4–9]. For UV photodetectors, fast response and recovery times and high responsiveness are commonly desired characteristics. A very short recovery time ranging from a few milliseconds to several seconds is commonly observed in UV photodetectors based on a single ZnO nanowire [9–11]. However, the single-nanowire UV photodetector is hard to be manipulated and measured, due to its small size and very low photoresponse current. To meet the requirement of real-time device application, many methods to enhance UV photoresponse current have been investigated [12, 13]. Li et al. reported a UV detector based on a ~3-□m-thick disordered ZnO NW film with a photocurrent of about 100 A [14]. Bai et al. fabricated a UV sensor by integrating multiple nanowires connected in parallel, achieving about 1-mA photocurrent [15]. But, in these studies of UV photodetectors based on ZnO NW arrays or multiple nanowires, the response and recovery times are too long, ranging from a few minutes to several hours [16–18],

which could be influenced by a number of factors at interplay, such as the nanowire surface [16], defects [17] and processing conditions [18].
In this study, we fabricated a simple and functional UV photodetector based on ZnO NW arrays grown on GaN thin films, achieving success in obtaining a considerable photocurrent and ultra-fast photoresponse and recovery times. Two indium tin oxide (ITO) electrodes were contacted with the top of the ZnO NW arrays, instead of expensive lithography and thermally evaporated metal contact pad processes. Our study shows that the well-crystallized ZnO NW arrays with fewer defects and a ZnO/GaN heterojunction lead to ultra-fast photoresponse and recovery times.

2. EXPERIMENTAL

Synthesis of the ZnO NW arrays was carried out by chemical vapor transport method deposition using a simple horizontal tube furnace. A gold catalyst layer with nominal thickness of 3–5 nm was firstly deposited on the *c*-plane GaN/sapphire substrate. The feedstock source materials consisting of a mixture (1:1 by weight) of ZnO and graphite powders were loaded in a quartz boat at the center of the furnace. Flows of 1 sccm oxygen (purity 99.999 %) and 49 sccm argon (purity 99.999 %) were used as the precursor and carrier gases, respectively. The chamber was heated to 950 ˚C at a rate of 50 ˚C/min. The whole process was held for 30 min under a constant pressure. Afterwards, the furnace was turned off and cooled to room temperature while maintaining the vacuum unchanged.
After growth, the morphology features of as-deposited products were characterized by means of a Sirion 200 field emission scanning electron microscope (FESEM). Raman spectroscopy was employed on a Jobin-Yvon HR800 microspectrometer in backscattering geometry to investigate the lattice vibrational properties of the ZnO NW arrays, with excitation source an argon-ion laser (λ 515 nm). A photoluminescence (PL) measurement was implemented on a LabRam HR UV spectrometer using a 20-mW He–Cd laser (λ 325 nm). UV photoresponse measurement was carried out between two ITO electrodes at a fixed bias volt- age of 5 V by switching the light from a portable UV lamp (λ 365 nm, 0.3 mW/cm^2) ‘on’ and ‘off’. The distance be- tween the sample and the UV lamp were fixed. All of the measurements were carried out at room temperature in ambient condition.

3. RESULTS AND DISCUSSION

While keeping all other growth parameters unchanged, including the powder source temperature, the substrate position, the carrier gas flow and the system geometry, the re- actor pressure changed and resulted in very different yield and morphology of ZnO nanostructures [19, 20]. The as- grown ZnO nanostructures exhibit a pearly blue color, covering the entire surface. The FESEM images in Fig. 1 exhibit the general morphologies of four samples grown un- der constant oxygen volume percentage (2 %) but variable chamber pressure. In sample 1 (S1) under the lower pressure of 100 Pa, the ZnO NWs were less well aligned. As the chamber pressure increases to 500, 1000 and 2500 Pa, ZnO NWs (samples S2, S3 and S4, respectively) were all vertically aligned well with respect to the substrate, having a fairly uniform length and distribution density. The aver- age diameters of the resulting ZnO nanowires were about 39, 75, 98 and 153 nm, respectively. Furthermore, the statistical distribution of the nanowires’ diameter was investigated. When the pressure increases, the standard deviation of the nanowires’ diameter increases, from 9.89, 13.8, 13.9 to 26.2 nm, respectively. However, by further increasing the system pressure to 3500 Pa, only random networks of nanowires were found instead of vertically aligned arrays. Above all, our experiment demonstrated that the chamber pressure is a very

important factor which has an effect on the growth, size and morphology of ZnO NW arrays. Only un- der a suitable range of stable pressure (500–2500 Pa) could a large area of uniform, vertically well-aligned ZnO NW arrays be synthesized using a catalyst-assisted hetero-epitaxial carbothermal reduction approach on a GaN substrate.

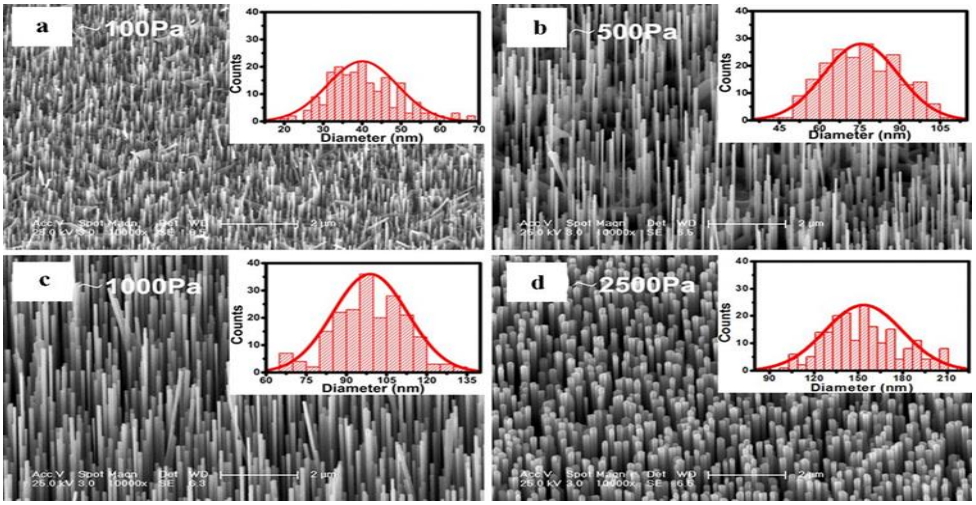

Figure 1 Typical FESEM images of ZnO NW arrays grown on GaN substrates at various chamber pressures.

It is worth mentioning that the optical properties of well- ordered ZnO NW arrays are further studied by the visible Raman spectrum, as shown in Fig. 2. Apart from the pho- ton modes of the underling sapphire and GaN template, here the remarkable, intrinsic E_{2H} mode of ZnO NW arrays has many features. The E_{2H} mode peak, assigned to oxygen atom vibration motion in samples S1–S4, is found at 438.5 0.5 cm^{-1} with a small FWHM range of 6.5–7.6 cm^{-1}. These mean that there is almost no stress in our 1D ZnO arrays [22]. A much-suppressed peak at 332.7 cm^{-1} is attributed to the second-order nonpolar Raman processes (E_{2H}–E_{2L}), assigned as E_2(M) in Fig. 2, which could be found only when ZnO is single crystalline. Hence, the pres- ence of a dominant narrow E_{2H} mode and a much sup- pressed E_2(M) mode in all cases confirmed the wurtzite hexagonal phase and very good crystal quality in the as-grown ZnO NW arrays.

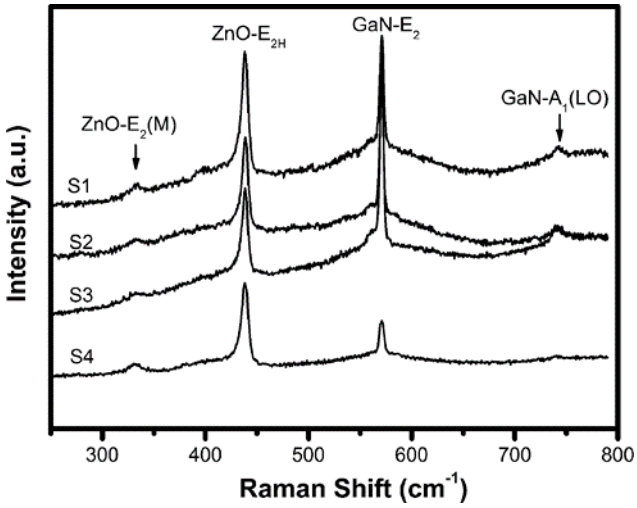

Figure 2 The Raman spectra observed from ZnO NW samples S1–S4 under 514.5-nm laser light excitation.

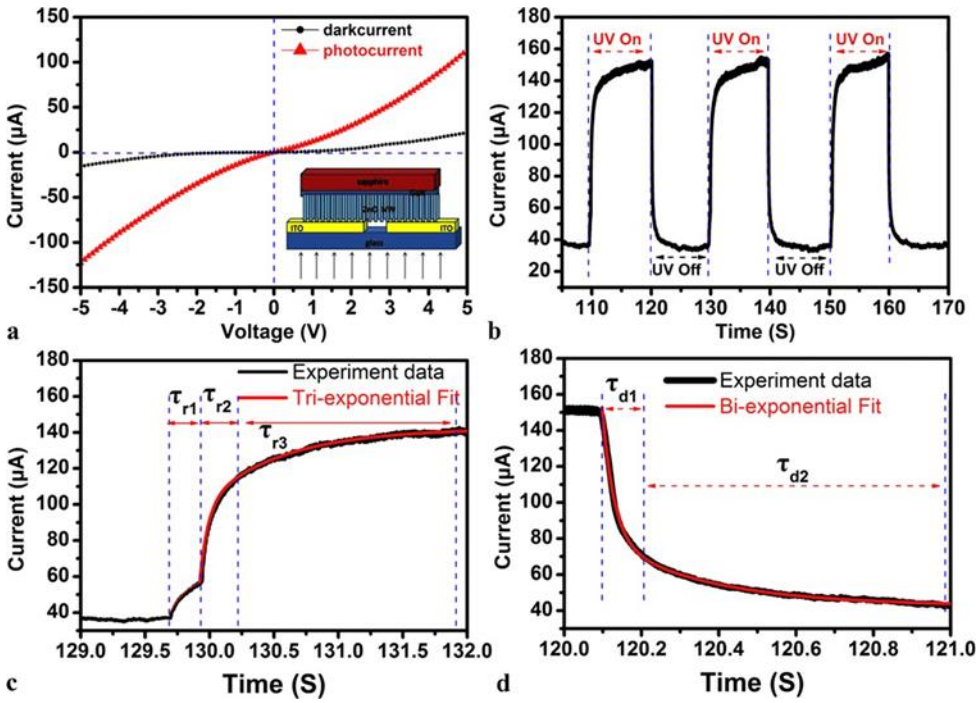

Figure 3 (a) I–V curves of the integrated sensor of ZnO NW arrays with and without UV illumination. Inset is the schematic of the fabricated NW photodetector. (b) Photoresponse of the NW UV sensor under a bias voltage of 5 V, 365-nm UV irradiation of 0.3 mW/cm^2. (c) Experimental (black line) and tri-exponential fitting (red line) curves of the photocurrent increase process. (d) Recovery current (black line) and the bi-exponential fitting (red line) curve of the UV sensor.

The structure schematic of the ZnO NW photodetector is shown in the inset of Fig. 3a. A ditch with width of 0.1 mm was firstly formed to separate two ITO electrodes. Then, the fabricated sample was reversed and placed on the prepared ITO/glass substrate. The tips of

the ZnO NWs are put in di- rect contact with the ITO/glass substrate to form the ZnO NW array device structure. This method needs neither de- positing any material on the NW tips to form contact elec- trodes nor passivating the surface of the ZnO NWs. Finally, polydimethylsiloxane (PDMS) was adopted to package the device. The UV response of our devices was characterized by a portable UV lamp at room temperature in ambient con- dition. The current–voltage characteristics of the photode- tector fabricated from sample S3 under dark and UV illumi- nation (365 nm, 0.3 mW/cm^2) are shown in Fig. 3a. The I–V curve was measured with bias from 5 to 5 V at room temperature in ambient condition. Clear rectifying behavior can nation. This phenomenon could be related to the large area and approximate ohmic contact between NW arrays and ITO electrodes.

At an interval of 10 s and a bias of 5 V, the photodetector can reversibly be turned 'on' and 'off' by switching the UV illumination, respectively, as shown in Fig. 3b. The on– off ratio is about 3.9. In Fig. 3c, the photocurrent initially grew very fast by two steps and then slowly increased and saturated at last. The photoresponse of the fabricated device shows a tri-exponential growth. The time-dependent growth behavior of the photoresponse curve is fitted with the equation As shown in Fig. 3d, after the UV light was turned off, the decay process was fast initially and then became slower. The decay time behavior follows a bi-exponential decay function. The UV response and recovery of ZnO NW are known to be generally governed by water molecules and ionized

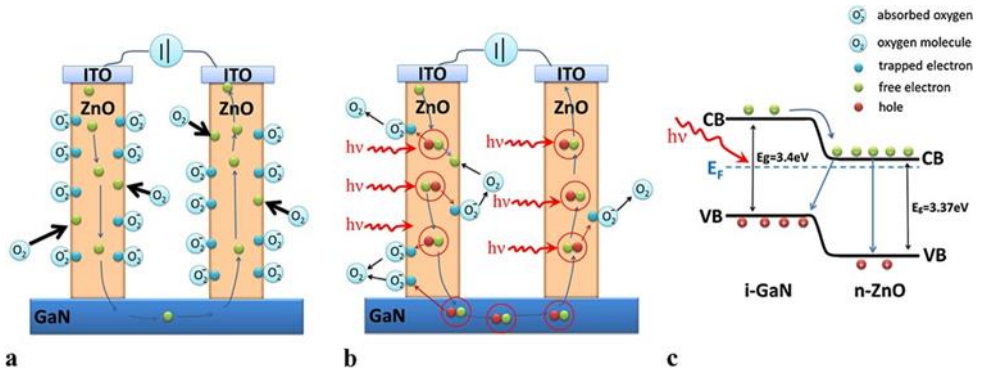

Figure 4 A schematic of photoresponse mechanism of the ZnO array photodetector. The electron transfer in the device at (a) dark condition and (b) during UV illumination, respectively. (c) Band diagram and transition process responsible for the hole–electron recombination at the ZnO/GaN heterojunction barriers

oxygen adsorption and desorption at the surface defect sites [23]. In the present case, as the ZnO NW arrays were grown at relatively high temperature, the influence of water molecules on the photoresponse was eliminated [16]. Oxy- gen is believed to play a critical role in the observed photoresponse. A schematic of the photoresponse mechanism of the ZnO NW array photodetector is shown in Fig. 4. In ambient conditions, oxygen molecules would adsorb on the NW. The density of electron–hole pairs in the ZnO NW and GaN thin film (band gap 3.4 eV) increases significantly when illuminated with 365-nm UV light. As the GaN thin film was covered by ZnO NW arrays, the density of absorbed oxygen molecules on the surface of GaN is rarely low. The holes in the GaN thin film excited by UV light would move to the ZnO NW surface across the ZnO/GaN heterojunction, then take part in the oxidization of the

ionized oxygen and release one oxygen gas molecule by an electron–hole recombination process, which is shown in Fig. 4b. This process may be the first part of tri-exponential growth with time constant τ_{r1} 0.148 s in the photocurrent increase curve. The second part of the tri-exponential photocurrent growth can explain by the process of the photon-generated holes in ZnO NWs, which will react with ionized oxygen at the surface. The well-crystallized ZnO NW arrays with fewer defects could increase the moving rate of holes, corresponding to a fast growth time constant τ_{r2} 0.064 s. However, the photocurrent cannot increase unlimitedly and will be balanced by the re-adsorption of oxygen molecules on the ZnO NW surface [24], leading to the photocurrent reaching the saturation value with a slow time constant τ_{r3} 0.613 s, as shown in the third part of the tri-exponential growth.

As the UV light turns off, the photocurrent shows an ultra-fast decay and then a very low decay. The ZnO/GaN interface shows type II band alignment, where both the valence-band (VB) top and the conduction-band (CB) bot- tom of n-type ZnO are located below those of i-GaN as shown in Fig. 4c. Therefore, during UV illumination, some holes from the GaN thin film are kept at the ZnO/GaN heterojunction for a junction barrier, instead of recombining with the electrons present in the ionized oxygen. As a result, these holes are available for recombination with the exciton-related free electrons at the heterojunction interface. During photocurrent decay, the ZnO/GaN heterojunction related electron–hole recombination dominates, which corresponds to the ultra-fast decay process in the photocurrent recovery with the time constant τ_{d1} 30 ms. Since the ad- sorption process of oxygen molecules is slower than the desorption process of photogenerated holes, the current decays and reaches the lowest value with a very slow process with the time constant τ_{d2} = 270 ms.

4. CONCLUSIONS

In summary, well-crystallized ZnO NW arrays were grown on GaN/sapphire by one-step chemical vapor deposition un- der control of the fabrication pressure of 1000–2500 Pa and the best-aligned arrays were obtained at 1000 Pa. A photo- luminescence study shows a red shift with nanowire diameter increase. Under 365-nm UV irradiation of 0.3 mW/cm2, the photoresponse study of the best ZnO NW arrays shows an ultra-fast tri-exponential growth with three constants of 0.148, 0.064 and 0.613 s, and a bi-exponential decay behavior with two recovery constants of 30 and 270 ms. The ZnO/GaN heterojunction barriers could be responsible for the ultra-fast tri-exponential growth and bi-exponential decay behavior.

References

[1] X.H. Zhang, L. Gong, K. Liu, Y.Z. Cao, X. Xiao, W.M. Sun, X.J. Hu, Y.H. Gao, J.A. Chen, J. Zhou, Z.L. Wang, Adv. Mater. 22 (2010) 5292
[2] Y.H. Gao, Y. Bando, Nature 415, (2002) 599
[3] X.F. Duan, Y. Huang, R. Agarwal, C.M. Lieber, Nature 421 (2003) 241
[4] M.H. Huang, S. Mao, H. Feick, H.Q. Yan, Y.Y. Wu, H. Kind, E. Weber, R. Russo, P.D. Yang, Science 292 (2001) 1897
[5] S. Jha, J.C. Qian, O. Kutsay, J. Kovac, C.Y. Luan, J.A. Za- pien, W.J. Zhang, S.T. Lee, I. Bello, Nanotechnology 22 (2011) 245202
[6] A.B. Martinson, J.W. Elam, J.T. Hupp, M.J. Pellin, Nano Lett. 7 (2007) 2183
[7] C.S. Lao, J. Liu, P.X. Gao, L.Y. Zhang, D. Davidovic, R. Tum- mala, Z.L. Wang, Nano Lett. 6 (2006) 263

[8] G.D. Yuan, W.J. Zhang, J.S. Jie, X. Fan, J.X. Tang, I. Shafiq, Z.Z. Ye, C.S. Lee, S.T. Lee, Adv. Mater. 20 (2008) 168
[9] G. Cheng, X. Wu, B. Liu, B. Li, X. Zhang, Z. Du, Appl. Phys. Lett. 99 (2011) 203105
[10] J. Bao, I. Shalish, Z. Su, R. Gurwitz, F. Capasso, X. Wang, Z. Ren, Nanoscale Res. Lett. 6 (2011) 404
[11] J. Zhou, Y.D. Gu, Y.F. Hu, W.J. Mai, P.H. Yeh, G. Bao, A.K. Sood, D.L. Polla, Z.L. Wang, Appl. Phys. Lett. 94 (2009) 191103
[12] K. Kwak, K. Cho, S. Kim, Nanotechnology 22 (2011) 415204
[13] B.O. Jung, D.C. Kim, B.H. Kong, D.W. Kim, H.K. Cho, Sens. Actuators B, Chem. 160 (2011) 740
[14] M. Mourad Mabrook, Exp. Theo. NANOTECHNOLOGY 2 (2018) 103
[15] S. Bai, W. Wu, Y. Qin, N. Cui, D.J. Bayerl, X. Wang, Adv. Funct. Mater. 21 (2011) 4464
[16] Y. Li, F. Della Valle, M. Simonnet, I. Yamada, J.J. Delaunay, Appl. Phys. Lett. 94 (2009) 023110
[17] A. Bera, D. Basak, Appl. Phys. Lett. 94 (2009) 163119
[18] Y. Wang, Z. Liao, G. She, L. Mu, D. Chen, W. Shi, Appl. Phys. Lett. 98 (2011) 203108
[19] R.F. Zhuo, H.T. Feng, J.T. Chen, D. Yan, J.J. Feng, H.J. Li, B.S. Geng, S. Cheng, X.Y. Xu, P.X. Yan, J. Phys. Chem. C 112 (2008) 11767
[20] X.D. Wang, J.H. Song, C.J. Summers, J.H. Ryou, P. Li, R.D. Dupuis, Z.L. Wang, J. Phys. Chem. B 110 (2006) 7720
[21] H. Zeng, G. Duan, Y. Li, S. Yang, X. Xu, W. Cai, Adv. Funct. Mater. 20 (2010) 561
[22] R. Cuscó, E. Alarcón-Lladó, J. Ibáñez, L. Artús, J. Jiménez, B. Wang, M.J. Callahan, Phys. Rev. B 75 (2007) 165202
[23] S. Dhara, P. Giri, Nanoscale Res. Lett. 6 (2011) 504
[24] S. Mridha, D. Basak, Appl. Phys. Lett. 92 (2008) 142111

Exp. Theo. NANOTECHNOLOGY 3 (2019) 95-101 https://doi.org/10.56053/3.1.95